Damage Location Sensing in Carbon Fiber Composites Using Extrusion Printed Electronics

Mohamad Kannan Idris[1], Paria Naderi[1], Garrett W. Melenka[2] and Gerd Grau[1]

[1] Electrical Engineering and Computer Science, York University, Toronto, Canada
[2] Mechanical Engineering, York University, Toronto, Canada

E-mail: grau@eecs.yorku.ca

Abstract

Structural Health Monitoring (SHM) uses sensors in advanced engineering structures to evaluate integrity and detect damage or deformation affecting structural performance, e.g., cracks, holes, or corrosion. Carbon fiber textile composites are commonly used to reinforce structures such as aircraft, vehicles, or bridges due to their high tensile strength to weight ratio, chemical resistance, and thermal and electrical conductivity. Printing electronics on textiles is a scalable manufacturing technology combining the physical properties of textile materials with the added functionality of electronic elements making them self-sensing. Extrusion printing is a contactless digital printing method to print electrical conductors and passive circuit elements. This paper proposes to combine conventional carbon fiber composite manufacturing processes with printed conductors to create self-sensing carbon fiber textile composites. Damage is sensed by measuring resistance changes in a carbon fiber sheet. Contacts are extrusion printed directly on woven carbon fiber sheets using silver flake ink. A multiplexed Kelvin Double Bridge circuit is the read-out interface. This allows small resistance changes due to damage to be measured in a 4-point configuration. The circuit is connected to the printed contacts on the carbon fiber sheet through multiplexers to detect damage in different locations. This 2D digital sensor can detect the location and size of damage holes for SHM. The resolution of the sensor is controlled by the location and spacing of the silver electrodes, which were studied experimentally and by simulation. The resolution is 26 mm in the current direction and 16 mm in the orthogonal direction. The threshold of detectable damage is 4 mm^2. Simulation of the sensor as an isotropic 2D conductor shows good agreement with experimental results for the orthotropic fabric. The resultant sensing device could be integrated into many composite structures as one of its layers or simply printed on the surface to create smart structures.

Keywords: Structural Health Monitoring, Carbon Fiber Composites, Damage Sensors, Extrusion Printed Electronics

1. Introduction

Structural Health Monitoring (SHM) is the process of identifying deformation and damage in advanced engineering structures by creating a system that combines these structures with an array of multi-purpose sensors.[1] Health monitoring sensors collect data about the different aspects of the mechanical system to report its integrity over time. The damage-sensitive data extracted from the sensors' measurements, along with the statistical analysis of this data, determine the current health of the structure.[2] For long-term use in structures that accumulate damage due to aging and their operation environments, SHM is used to assess the ability of the structure to perform its function. SHM is used in many industries, including mechanical, civil, and aerospace, to monitor damage in both products and manufacturing infrastructure, where detecting damage has life-saving and economic impacts.[1, 3] In aerospace, SHM is used for real-time monitoring of aircraft integrity. If damage occurs, it could be found and reacted to instantly, thus increasing aircraft safety. Additionally, SHM reduces the time on the ground needed for traditional inspection methods, thus increasing operation time and potentially lowering costs.[4] In civil infrastructures, in addition to providing a continuous assessment of the integrity of bridges and buildings, SHM is used for safety assessments of

the structures after disasters and extreme events such as earthquakes, and it provides immediate instructions for planning maintenance and repair.[1, 5]

Generally, damage can be defined as an alteration introduced to the structure that affects its performance, such as holes, cracks, or corrosion.[2] SHM operates when damage or deformation occurs in the structure. It is achieved using a system that compares the damage state of the structure to a previous undamaged state.[1] The damage significantly changes a physical property in the system, which alters the measurement response of the system. However, this premise faces various challenges, mainly, that damage is usually localized and may not have a significant effect on the overall measurement response of the system. Another challenge SHM faces is defining the possible damage types that may occur to choose a suitable sensing system. Also, it must be shown that the sensor itself is not damaged before field deployment.[1]

In the past decade, sensing technology has made significant progress, and different types of sensors are becoming commercially available.[5] Ultrasonic SHM sensors transmit and receive waves that follow a waveguide and thus measure with high sensitivity the geometrical changes in the structure. Such sensors suit large stationary structures such as bridges due to their low attenuation over large propagation distances.[6] Piezoelectric wafer active sensors use the Electro-Mechanical Impedance Method to detect damage on structures.[2, 7] They could be permanently mounted on structures such as aging aircraft to monitor fatigue cracks and corrosion.[8, 9]

SHM sensors are of interest for integration into textile composites. Textile composites are engineered materials that combine the unique physical properties of their multiple components.[10] Most prevalent among textile composites are carbon fiber (CF) composites that are commonly used to reinforce structures such as aircraft, vehicles, bridges, and other concrete structures. Carbon fiber has a wide variety of desirable properties, including high tensile strength to weight ratio, chemical resistance, and thermal and electrical conductivity, which can be tailored as desired, enabling a wide range of applications. Carbon fiber composites are currently available in industries such as aerospace, athletics, construction, automotive, defense, marine, and wind energy.[11]

SHM sensors within textile composites will allow for the capability of in-situ wide-area sensing, and they can be integrated with common manufacturing processes. Integrated SHM sensors create multi-functional textile composites that can monitor and diagnose their health states.[12] Carbon fiber composites are being used as piezo-resistive sensors for SHM embedded in structures such as concrete and glass windmill blades.[13–21] These studies embed single fibers or yarns in structures, thus, the sensing is limited to the direction along the fibers. Another report has used carbon fiber fabric as capacitive electroluminescent sensors for wider area sensing on structure surfaces.[22] For composites that are naturally conductive such as carbon fiber composites, electrical resistivity tomography (ERT) detects the location of damage in composite sheets by measuring resistance between different points on the sheet. This method has been demonstrated in various configurations with different electrode arrangements and composite types. ERT has been studied for carbon fiber reinforced polymer (CFRP) most commonly for unidirectional CF [23] and cross-ply laminate layups of multiple unidirectional layers,[24–28] as well as in a limited number of studies for woven textile composites.[29–31] Whilst these reports have demonstrated good damage detection, the electrical contacts have generally been fabricated by non-automated methods that are difficult to scale such as razor blade contacts,[23] copper foil embedded in the CFRP,[25] manual attachment of wires using conductive adhesive,[24, 26, 27] or attachment to a printed circuit board (PCB) using silver paste.[30] These methods also often require removal of the cured epoxy resin on top of the carbon fibers using techniques such as milling, sandblasting, laser irradiation, or chemical cleaning to ensure low resistance between the contact material and the carbon fibers.[30]

A promising method to fabricate metal contacts in a low-cost fashion that can be scaled to large structures is printing. Printing is promising because it can be low cost, low weight, mechanically flexible, and ecofriendly. In addition, digital printing processes for electronics are scalable and allow for on-demand printing, which makes printed electronics a critical technological enabler for the Internet of Things (IoT).[32] Printing electronics on textiles combines the physical properties of the textile materials with the added functionality of the electronic elements.[33] However, printing methods face multiple challenges when used with textiles, namely, the high surface roughness and porosity of the textiles. Various printing techniques have been used to print electronics on textiles, including inkjet printing, screen printing, and extrusion printing.[34]

Printing of contacts has been demonstrated on CFRP pre-impregnated with epoxy resin (prepregs) to monitor strain and surface cracks using resistance measurements during bending tests. One report uses strips of CFRP with inkjet printed silver lines along the strip and measures the resistance of the CFRP in the different locations to determine the location of strain and damage.[35] Another report uses CFRP in the shape of an aeronautical stiffener and inkjet prints silver contacts in strategic locations to measure the change of resistance due to bending in a diagonal direction.[36] The adhesion between inkjet printed silver on top of and in between carbon fiber composite layers has been studied experimentally and numerically.[37–39] The contact resistance between unidirectional prepregs and blade printed silver or copper was studied for different polishing methods to remove the epoxy.[40, 41] These previous studies were performed on unidirectional fiber composites or layups and sensing was only performed along one direction. Conversely, woven textile composites have the advantage of having two symmetry axes, both mechanically and electrically, which allows determining the location of damage in two dimensions. However, woven textiles generally have a low overall electrical resistance due to the good contact between interwoven

orthogonal fibers and are therefore more prone to measurement errors caused by contact resistance.[29] This means contact fabrication is especially critical. Although electronic textiles (e-textiles) can be manufactured in various ways such as sewing and knitting, braiding, weaving, chemical treatment, and coating/laminating, printing is the most promising due to the previously mentioned advantages of the process.[42] Here, we propose a method using extrusion printed contacts to use the carbon fiber textile itself as the sensing element and convert it into an e-textile that senses and determines the location of a damage in two dimensions.

Extrusion printing, also known as dispense printing, is a contactless nozzle-based printing method. It is digital, which means ink is extruded only when needed and does not require any lithography masks or printing master. It works by applying pressure in an ink cartridge to dispense ink through the nozzle. Extrusion printing can be used to print stretchable and flexible conductors and passive circuit elements.[43, 44] Highly viscous inks are used in this process (approximately 10^3 to 10^6 cP) to prevent leakage through the nozzle.[45] This creates thick-layer patterns, which makes this process ideal for printing on textiles. Metal-based inks are the most commonly used inks in extrusion printing of electronics, such as silver ink made from silver flakes and a polymer binder dissolved in a solvent.[46] Compared to other printing methods such as screen printing and inkjet printing, extrusion printing combines the desired attributes for printing on textiles. Extrusion printing uses high-viscosity paste, which does not spread uncontrollably when printed onto porous and rough surfaces enabling printing onto untreated carbon fiber fabrics. In contrast, inkjet printing uses much lower viscosity inks, which means well-defined patterns require printing onto well-controlled surfaces. Extrusion printing is also less prone to nozzle clogging, which can reduce manufacturing reliability and yield with inkjet printing, especially for large areas as can be found in many CFRP applications. In contrast to screen and blade printing, extrusion printing is a digital, print-on-demand technique that does not require a mask. Therefore, circuit patterns can be easily adapted for research, design, or manufacturing of new geometries.[47, 48] The main challenge of extrusion printing on textiles is that this method requires the nozzle to be close to the substrate for continuous printing. The proximity of the nozzle to the textile substrate results in the nozzle entangling in the fibers of the textile which could break the nozzle and move or damage the textile. This challenge was overcome in our previous work and extrusion printing allows electrodes to be printed on woven carbon fiber in strategic places.[49] Here, these electrodes are connected to a read-out circuit, and are used to inject current through the composite and measure small changes in voltage. Measuring the changes in voltage in specific locations in the carbon fiber composite enables detection of damage inflicted on the composite and detection of the damage location.

This paper proposes to use woven carbon fiber textiles as the primary sensing element without significant changes to conventional CFRP manufacturing processes with the addition of extrusion printing of silver flake ink, which has not been reported before. Previous work used manual deposition of contacts, which is not scalable and precise, blade coating/ printing, which is difficult to adapt to new and complex geometries, or inkjet printing, which is not compatible with the rough surface of untreated carbon fiber fabrics. Extrusion printing overcomes these challenges of previous contact fabrication methods. The main open question that is addressed here is whether scalable printing technology can create electrical contacts on a woven carbon fiber composite of sufficient quality to detect damage in the composite. This paper presents the design, manufacturing, and characterization of a 2D wide-area self-sensing woven carbon fiber composite utilizing extrusion printed contacts. Different contact pattern designs are studied, which is enabled by the fact that extrusion printing allows the precise deposition and fast re-design of circuit patterns. This was combined with a multiplexed Kelvin Double Bridge circuit to detect small resistance changes, which was applied to the detection of damage in carbon fiber composites for the first time here. It can detect different sizes of holes as damage for structural health monitoring of composites. The resultant sensing device could be integrated into many structures as one of its layers or simply applied to the surface.

2. Methods

2.1 Materials

The printing pattern was designed using EAGLE, Autodesk. The extrusion printer was a desktop printed circuit board printer (Voltera V-One PCB printer, Kitchener, ON). The conductive ink contains silver flakes in a thermoplastic polyurethane resin and a solvent (120-07 from Creative Materials Inc.), which has a viscosity (26,000 - 30,000 cP) high enough for extrusion printing. The flake size is in the range of 1-5 µm. The resistivity of the printed silver is $3*10^{-5}$ Ω.cm. The nozzle size was 225 µm. A low temperature (<205 °C) solder wire from VOLTERA was used to solder copper wires to the silver in the carbon fiber composite.

All carbon fiber fabrics were acquired from Sigmatex Ltd. The type used was polyacrylonitrile (PAN) derived 3K twill fabric. These fabric has 3,000 fibers each with 7 µm diameter in each tow. The electrical resistivity of a single carbon fiber extracted from the fabric was measured ($\rho = 2.37*10^{-3}$ Ω.cm) using the 4-point probing method [50] and by measuring the fiber diameter using an optical microscope. However, this resistivity does not capture the behaviour of the fabric due to its complex

structure. A device that models one section (sensing unit) of the damage sensor was designed as shown in Figure 1 (a), and multiple samples were manufactured using the same manufacturing steps described below. The resistance was measured using both the 2-point and 4-point methods for comparison. The results are reported in Table 1. The 2-point probe method gave inconsistent and much larger values, which means 4-point measurement is required. Finally, a cross section of the device was cut using a precision diamond wire saw (DWS 100, Diamond WireTec, Weinheim) and the thicknesses of the carbon fiber fabric, silver and epoxy were measured using a microscope as shown in Figure 1 (b) and (c). These results were used to calculate the resistivity and sheet resistance of the carbon fiber fabric ($\rho = 7.85*10^{-3}$ Ω.cm and $R_s = 0.27$ Ω/sq) as described in the supplementary information. The resistivity for the woven sheet is approximately three times the value for a single carbon fiber. This could be due to the non-conducting epoxy filler in the fabric, the contact resistance between fiber bundles in the fabric, or limited depth of current penetration. The effects of these factors are difficult to distinguish, and the measured resistivity should be viewed as an effective resistivity for this 2D carbon fiber sheet. This sheet resistance describes the behaviour of the 2D device and is the quantity that is measured to determine damage. Introducing damage to the device here means that carbon fiber bundles are cut throughout the entire thickness of the sheet (puncture damage), conductive material is removed, and consequently the value of this sheet resistance increases. In turn, this changes the voltage values measured enabling the sensing mechanism of the damage sensor device.

The epoxy infused into the fabric was the 2000 laminating epoxy resin system 9 from Fibre Glast (2000 epoxy resin and 2020 hardener), which is a room temperature two-part system. The viscosity of the mixed epoxy resin is 950-975 cP. The epoxy was mixed in the recommended weight ratio (4:1 Resin: Hardener). Polished stainless-steel plates were used as molds to give the composite its final flat shape and a smooth surface finish. LOCTITE Frekote 700-NC was used as a release layer on the plates to create multiple interfacing layers that prevent the epoxy from sticking to the plates.
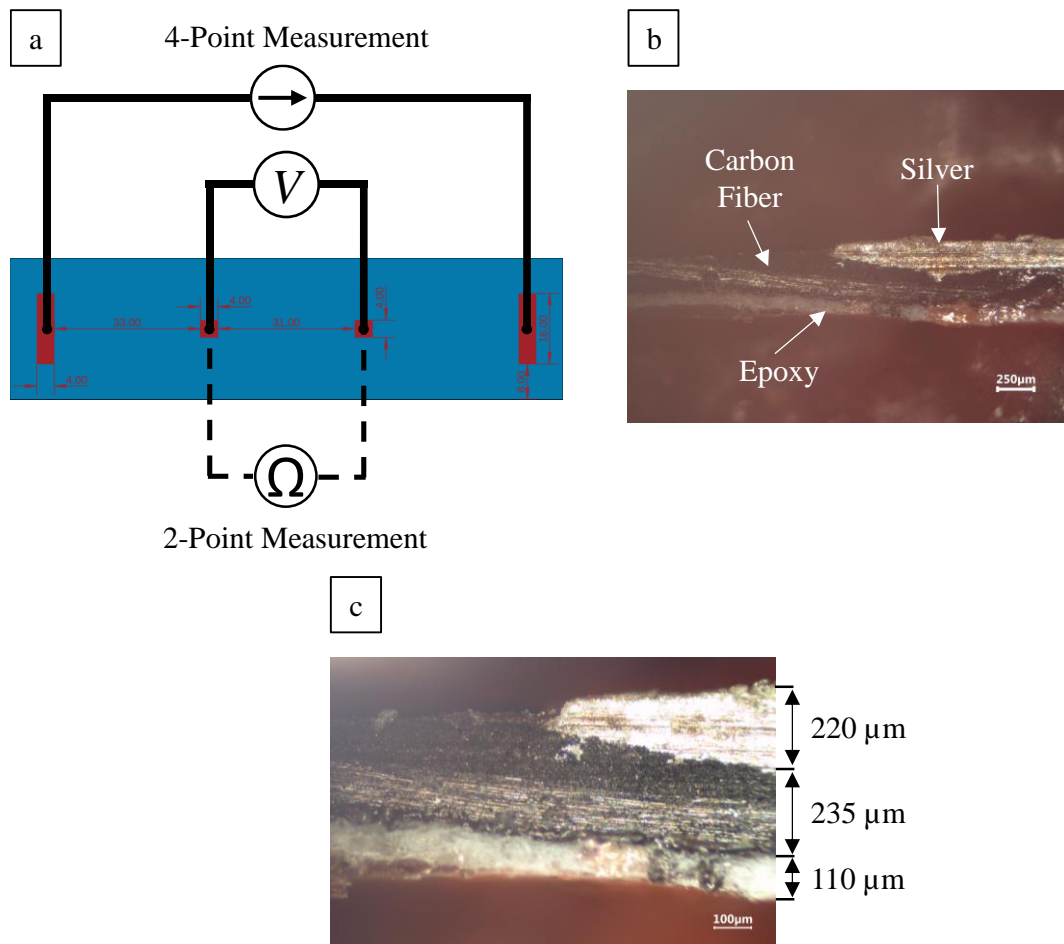

Figure 1. a) Design of one-section sensor device (one sensing unit) showing the measurement connections of the 4-point measurement (top) and the 2-point measurement (bottom). b) Cross section of the corner of the silver contact in the carbon fiber sensor device in an optical microscope showing the three layers: silver, carbon fiber and epoxy. c) A magnified image of (b) showing the thickness of the layers.

Table 1. Resistance measurements (Ω) of one section device samples using both 4-point and 2-point measurements. The 4-point measurements show a consistent result unlike 2-point measurements.

Sample	#1	#2	#3
2-Point	1.8	3.3	2.5
4-Point	0.267	0.264	0.266

2.2 Printing on Carbon Fiber

The V-One printer has multiple operation phases: probing, ink calibrating, and printing. In the probing phase, a metal needle contacts and probes multiple positions on the substrate to be printed on and measures height and position using a set of sensors. This phase is essential because it ensures that the nozzle tip does not contact the substrate and does not break in the printing phase, and it ensures consistency in printing. In the ink calibration phase, the ink cartridge is mounted on the dispenser, and a built-in calibration design is printed on the substrate. In this phase, the printing parameters can be optimized until the printing reaches the desired amount of dispensed ink. The most important printing parameters are nozzle height, kick, rheological setpoint, and feedrate. Nozzle height represents the distance offset of the nozzle from the substrate. Kick controls the stroke length of the dispensing piston relative to its position at the time. The rheological Setpoint parameter corresponds to the way the dispenser compensates for pressure loss in the cartridge. An increase in rheological setpoint results in an increase in ink flow rate over time. Together kick and rheological setpoint control the amount of dispensed ink by controlling the pressure in the ink cartridge. Feedrate controls the nozzle XY-axis movement speed during ink dispensing. It is necessary to find the optimal combination of these parameters to ensure smooth continuous printing. Finally, in the printing phase, pressure inside the cartridge is applied using a piston while moving the nozzle around; thus, printing the desired pattern on the substrate.

Extrusion printing on carbon fiber fabric using the V-One printer presents multiple challenges. Firstly, the contact-based probe is not suitable to be used with textiles. When probing, the needle can bend and break the fibers, or the probe penetrates between the fiber tows. To avoid this, only the underlying glass holder was probed, and the thickness of the carbon fiber fabric was added and assumed to be constant. Secondly, the carbon fiber fabric has an uneven surface topography and could have frayed fibers and tows that could easily become entangled with the nozzle. An additional height offset of 350 μm was added to the nozzle height to overcome the variations in the surface height of the woven carbon fibers. This height offset was the minimum offset that allowed safe printing on the carbon fiber fabric. In addition, the fabric was secured on the glass substrate, which creates a small amount of tension on the fabric. Then, the fabric was sprayed with acetone, which mechanically pushes down the frayed fibers and tows and sticks them to the glass under it by surface tension. Finally, the drastic increase in nozzle height decreases the amount of ink dispensed per unit length. As a result, the other printing parameters had to be adjusted to reach optimal ink dispensing for printing. The printing parameter values used were: nozzle height offset 350 μm; kick 0.5 mm; rheological setpoint 0.5; feedrate 500 mm/min. Further details of the extrusion printing process on carbon fiber can be found in.[49]

2.3 Device Manufacturing

The sensor device was manufactured in four steps, as shown in Figure 2. In the first step, as shown in Figure 2 (a), (b), the desired silver pattern is printed on a dry carbon fiber fabric using the printing method described above. Then, the silver was cured in a gradually heating oven at 200 ℃ for 60 minutes. After removing the fabric from the oven, it was infused with the epoxy resin (Figure 2 (c)) and sandwiched between two polished stainless-steel plates that acted as molds for the final flat shape. Pressure was applied on the plates (3 tons of force) using a mechanical press (MAXIMUM 10-Ton Shop Press). This compression curing ensures a smooth surface finish and provides compaction to the woven yarns, as shown in Figure 2 (d). Due to the press force, the carbon fiber and the silver contacts get compressed, and the silver contacts become embedded in the carbon fiber. This is shown in Figure 1 (b) and (c). The composite was left in this state to cure for 24 hours at room temperature. Next, the composite was delaminated from the steel plates. The epoxy covering the silver electrodes was burnt off using a soldering iron at 450 ℃. Jump wires were then soldered to the electrodes to be able to connect them to the breadboard and the rest of the circuit as shown in Figure 2 (e). In the future for commercial manufacturing, soldering of the jump wires can be replaced with silver interconnect lines printed onto the CFRP. The printed contacts that are in direct contact with the carbon fibers are the focus of this proof-of-concept study as they are most critical both in terms of contact resistance and printing onto a rough surface. Future interconnect lines only need to make electrical contact with the already printed silver contact pads and printing onto smooth epoxy is a simpler process. There may be a contribution to contact resistance from the copper wire, solder and their interfaces (see Figure 2 (f)), which will be removed by the Kelvin Double Bridge interface circuit described below.
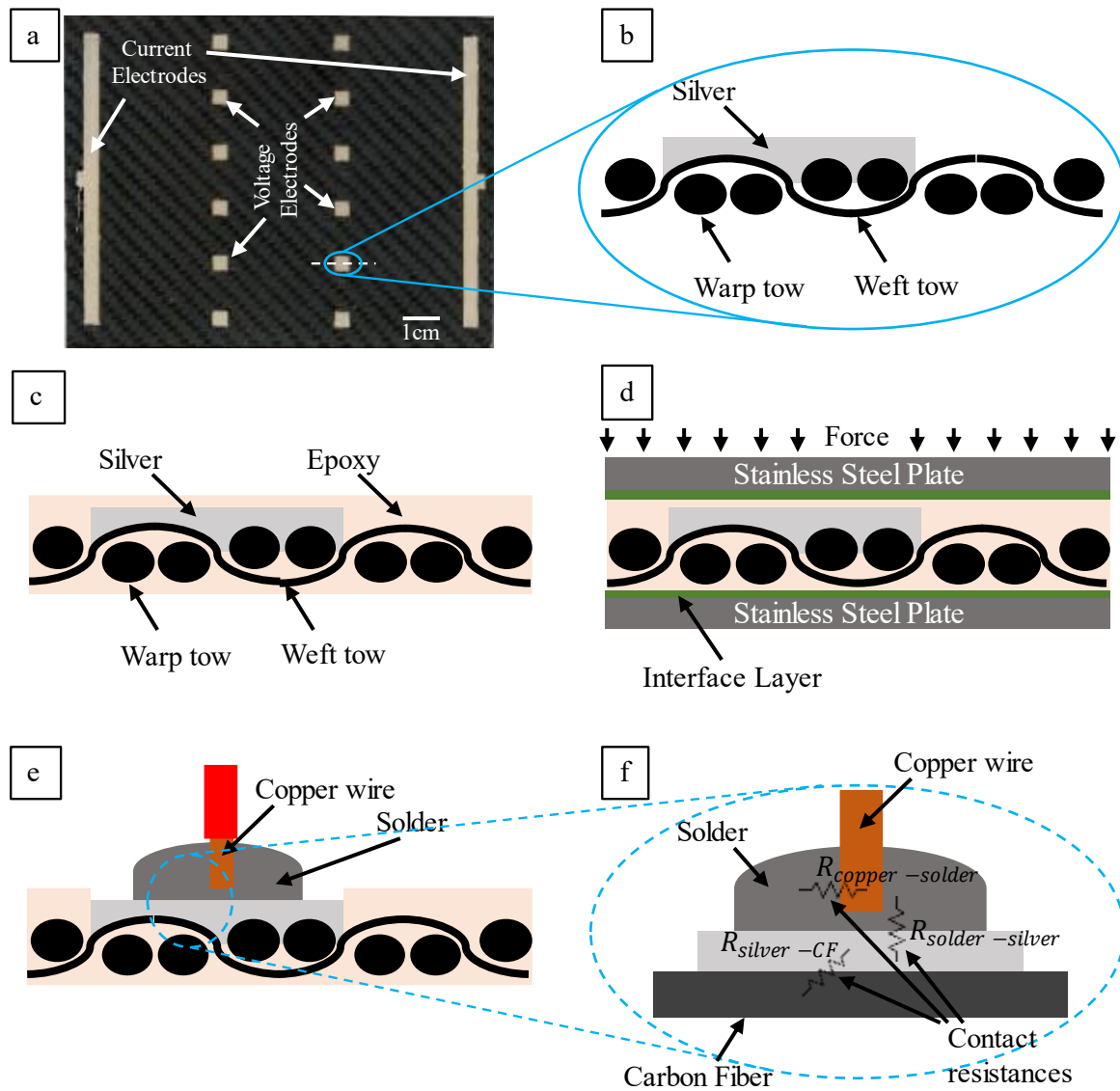
Figure 2. Manufacturing steps of the carbon fiber damage sensor using 3K twill carbon fiber woven fabric, epoxy resin, and silver ink. a) Photo of carbon fiber fabric with printed contacts. Long bars are used for current injection. Smaller square electrodes are used for voltage measurement at different positions to locate damage. Illustration of manufacturing steps of carbon fiber damage sensor: b) Cross-sectional view of printed contacts on carbon fiber. c) Infusing carbon fiber fabric with epoxy resin. d) Curing under pressure from mechanical press. e) Burning the epoxy off silver pads and soldering copper wires to them, which creates a series of contact resistances shown in (f).

2.4 Measurement and Data Acquisition Circuit

A circuit was created to collect and process the electrical measurements from the carbon fiber composite. The circuit combines the Kelvin Double Bridge 4-point probing method, digital multiplexing, and a data acquisition (DAQ) unit, as shown in Figure 3. To measure small impedance variations in piezo-resistive sensors, a Wheatstone bridge circuit is commonly used.[51] The Kelvin Double Bridge is an alteration of the Wheatstone bridge that includes an extra set of ratio resistor arms that provide higher measurement accuracy and enable the detection of even smaller resistance variations.[52] The six resistors of the Kelvin Double Bridge shown in Figure 3 are $R_1, R_2, R_3, R_1', R_2'$ and the carbon fiber composite (R_x). The resistance of the carbon fiber fabric was measured using a DC current-voltage source measure unit (KEITHLEY 2602B SYSTEM SourceMeter®) in both 2-point and 4-point configuration. This unit was also used as a constant current source (100 mA) when the Kelvin Double Bridge circuit was assembled. Using 2-point measurement, the resistance of the carbon fiber from the top voltage electrode to its corresponding bottom voltage electrode was approximately 2 Ω. Using 4-point measurement, the resistance decreased to an average of 0.5 Ω. Therefore, the total contact resistance is about 1.5 Ω. Resistor R₃ is chosen to have a similar resistance to and approximately balance the expected resistance of the carbon fiber sensor (1 Ω) to minimize the DC component of the measured voltage signal. The resistors R_1, R_2, R_1', R_2' are set to a high value (5.6 kΩ) to prevent current from flowing through them and are used for voltage measurement, thus, removing the effect of any contact and extra resistance introduced between the measurement point and the carbon fiber following the 4-point probing method.[50] The resistance of the carbon fiber device under test (R_x) can be calculated from the measured voltage V_G using formula (1). The derivation of this formula can be found in the supplementary information.

$$R_x = 2\frac{V_G - V_{G|(R_x=0)}}{I} \qquad (1)$$

I is the current supplied by the current source. $V_{G|(R_x=0)}$ is the measured voltage when a short circuit with zero resistance is measured instead of the carbon fiber device for calibration. Digital multiplexers are introduced to switch between electrodes and measure all possible combinations of voltage difference between the top and the bottom rows of electrodes. The multiplexers are in the voltage measurement line and have a low on-resistance compared with R_1, R_2, R_1', R_2' so that they do not affect the measurement result, just like contact resistance. The multiplexers used (ADG506AKNZ) have 16 channels, which is sufficient to study different sizes of the sensor sheet. The multiplexers were controlled using a small microcontroller (Arduino – UNO). Finally, a 12-bit DAQ unit (NI USB-6210, National Instruments) was used to measure the voltage with high accuracy and collect data in real-time. Both the microcontroller and DAQ were controlled simultaneously using a computer and programmed using MATLAB. In a future real-world implementation, both the microcontroller and the DAQ could be replaced with an application-specific integrated circuit (ASIC). The circuit was assembled using a breadboard and copper jump wires that were soldered to the printed silver contacts in the carbon fiber sheet.

To test the damage sensor, it was connected to the circuit and measured in the undamaged state. The measurement consists of the voltage differences between each electrode from the top row of voltage electrodes and its corresponding electrode from the bottom row. Each measurement was acquired 50 times to minimize measurement error using a loop in the program, and the average of these measurements was the value used for analysis. The damage was applied by drilling holes of various sizes within the sensing area into the composite. The drill used was a SKIL 3320 10-Inch Drill with a 5/64" drill bit at 3050 RPM. To make sure the drilling only affects the carbon fiber fabric itself and not the printed contacts, 2-point and 4-point resistance measurements were taken before and after damage was introduced to the sample shown in Figure 1 (a). The measurements show that contact resistance does not change with drilling as shown in Table S1. After damage was applied successively, the electrical measurements were taken again in the same manner and the mean of each set of 50 measurements was compared to its corresponding value before damage was applied.
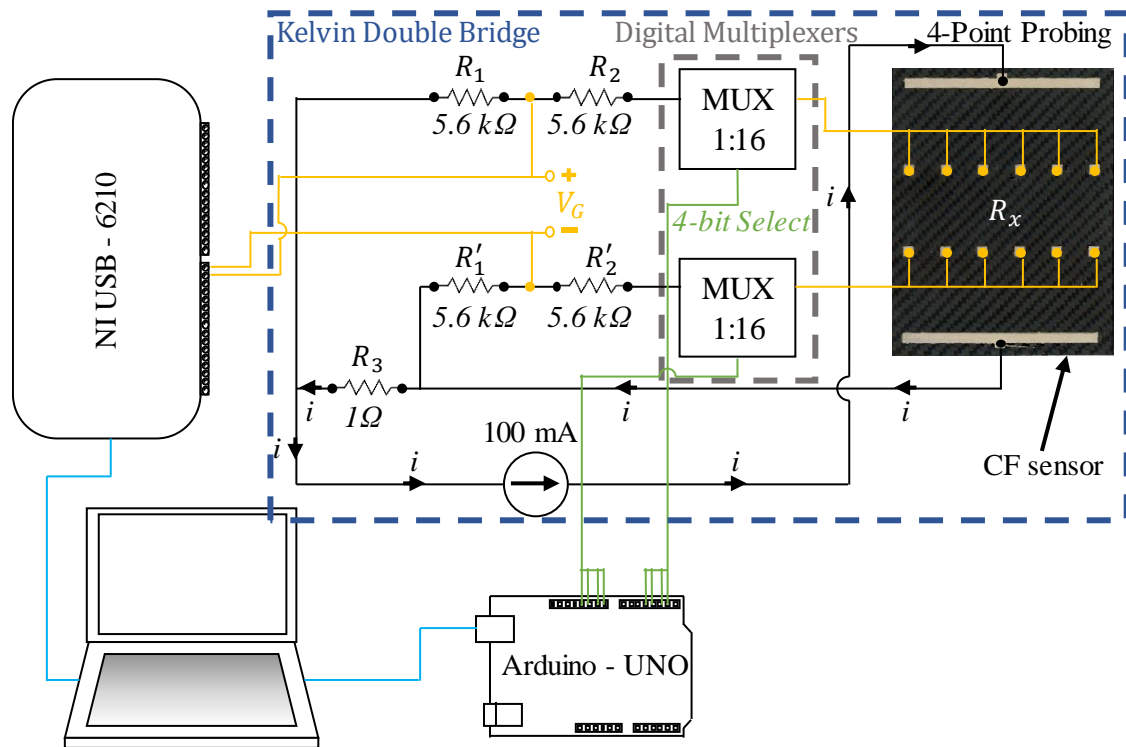
Figure 3. Circuit combining Kelvin Double Bridge, 4-point probing method, digital multiplexing and data acquisition tool (NI USB-6210) to automatically measure and record voltages in multiple locations on the carbon fiber (CF) sheet while canceling contact resistance.

2.5 Pattern Design and Simulation

The printing patterns were designed using EAGLE from Autodesk. Figure 4 (a) shows the dimensions of the 1-dimensional (1D) sensor where the damage location could be determined only along the width of the composite. Figure 4 (b) shows the alteration to make the sensor detect damage in two dimensions (2D). The top and bottom bus electrodes are where the current is injected. The rows of square electrodes in the middle are used to measure the voltage across the carbon fiber sensing area. In the 2D design, the top and bottom row voltage measurements are taken relative to the middle row creating two sensing areas. Potentially, more sensing areas could be added by adding more rows of voltage electrodes and increasing the length of the carbon fiber. However, this experiment was limited by the printing area of the V-One printer. Different electrode designs were analyzed qualitatively using a lumped resistor model and simulated more fully using Sentaurus 2020.09 to calculate and visualize the electric potential as a function of position in the carbon fiber sheet. Silicon doped with arsenic was used as the conductive material to simulate the carbon fiber fabric. Changing the doping concentration of arsenic in silicon changes the electrical conductivity of the sheet. The doping concentration of arsenic in the silicon was chosen as $6.19*10^{18}$ cm^{-3}. This value was realized by sweeping the doping concentration value until a resistivity of $7.85*10^{-3}$ $\Omega.cm$ and sheet resistance value of 0.27 Ω/sq was achieved to match the measured values of the carbon fiber fabric. Silver was used to simulate the printed silver electrodes. Silicon dioxide (SiO_2), a perfect insulator, was used to simulate damage, as shown in Figure 4 (c). However, changing the electrical conductivity of carbon fiber, silicon in the simulation, has minimal effect on the final detection results for the sensor when voltages are normalized as discussed below in section 3.3. This model assumes it can be neglected that the carbon fiber sheet is not a simple uniform conductor but consists of woven fiber tows.
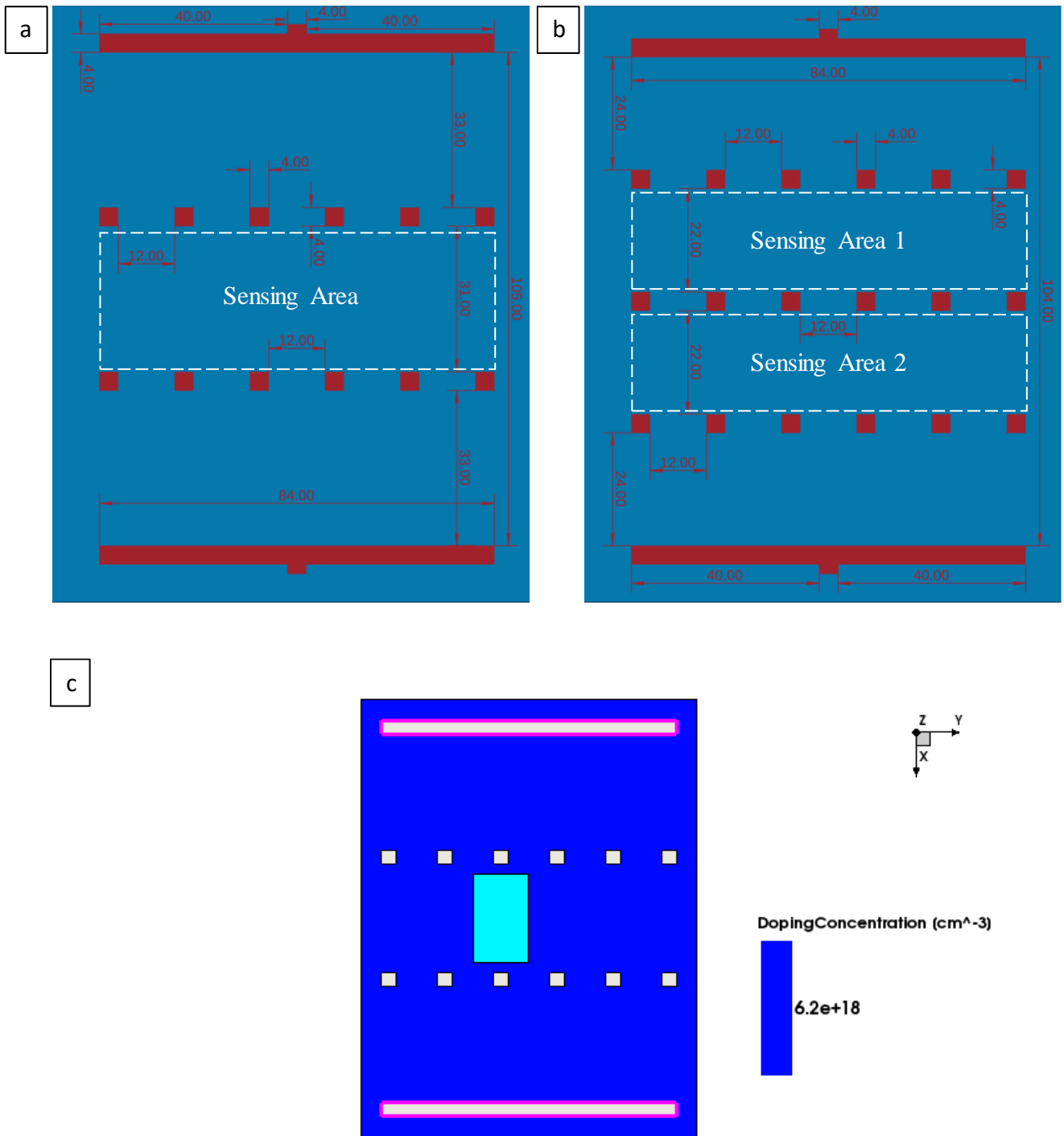
Figure 4. Printing pattern designs for carbon fiber damage sensors. a) EAGLE CAD design of 1D damage sensor. b) EAGLE CAD design of 2D damage sensor. Dimensions in (a) and (b) are in millimeters. c) Geometry of Sentaurus simulation of 1D damage sensor with damage introduced. Blue represents conductive carbon fiber; white represents electrodes; cyan represents non-conducting damage.

3. Results and Discussion

3.1 Sensor Pattern Design

When designing the sensor pattern, the main goal is to increase the sensing area as well as spatial sensing resolution. In order to get a first-order understanding of the underlying physics that informs design choices, a lumped resistor model was used to model the carbon fiber sensor. This model assumes that adjacent electrodes are connected by resistors. The model ignores the distributed two-dimensional nature of conduction in the carbon fiber sheet. Therefore, it only provides qualitative, not quantitative insights; however, these insights are valuable to gain an intuitive understanding for initial design choices. Quantitative modeling is performed using finite-element modeling, as described in section 3.3.

Figure 5 (a) shows the circuit representation of the carbon fiber sensor sheet. The nodes at the center of the circuit correspond to the voltage electrodes of the sensor. The nodes directly connected to the current source correspond to the current bus electrodes of the sensor. The resistors represent the carbon fiber fabric between the electrodes. The resistors R_{T1}, R_{T2}, R_{T3}, R_{B1}, R_{B2} and R_{B3} model the resistance between the current injection electrodes and the voltage electrodes. The resistors R_{T_1TO2}, R_{T_2TO3}, R_{B_1TO2} and R_{B_2TO3} model the resistance between the voltage electrodes. The resistors R_1, R_2 and R_3 model the main sensing area. The values of the resistors correspond to the physical distance in the pattern. The higher the resistance, the larger the distance between the electrodes. The process of developing this design has been done in three steps indicated as Design 1, Design 2 and Design 3. In Design 2, the values of R_{T1}, R_{T2}, R_{T3}, R_{B1}, R_{B2}, R_{B3} were increased and R_1, R_2, and R_3 were decreased compared to Design 1. In Design 3, the values of R_{T_1TO2}, R_{T_2TO3}, R_{B_1TO2} and R_{B_2TO3} were increased. The final values of R_{T1}, R_{T2}, R_{T3}, R_{B1}, R_{B2}, R_{B3}, R_1, R_2, and R_3 are 0.7 Ω, and the resistance values of R_{T_1TO2}, R_{T_2TO3}, R_{B_1TO2} and R_{B_2TO3} are 0.2 Ω. The process is described in detail in the supplementary information.

The value of R_1 is increased from its value before damage (No Damage: ND) to 100 kΩ, simulating damage (D) in the area between the voltage measurement electrodes. The voltage between the current electrodes increases, which corresponds to the increased overall resistance of the carbon fiber sheet due to the damage in the fabric. Results in Figure 5 (b). Design 2 shows an improved damage location detection compared to Design 1. The voltage across the damaged location 1 is now increased by 25% compared to the undamaged location 3 furthest from the damage. Design 3 shows further improvement for damage location detection by approximately another 30%. Figure 5 (c) shows the result in Figure 5 (b) normalized to values between 0 and 1 for the different electrodes. This normalization makes it easier to clearly pinpoint the location of the damage indicated with a value of 1.

In summary, increasing the physical distance between the current and the voltage electrodes as well as increasing the distance between the voltage electrodes in the same row increases damage location detection accuracy. However, the increase in physical distance between the current electrode buses and the voltage electrode rows results in a decrease in the active sensing area. Additionally, the increase in physical distance between the voltage electrodes in the same row means that fewer electrodes could fit in the space of the carbon fiber fabric, which is dictated by the application. This results in a decrease in the resolution of location-sensing as it is defined by the numbers of electrodes. Further quantification of the sensor voltage response requires a more complete consideration of the two-dimensional nature of the sheet, as shown in the following experimental results and finite-element modeling.
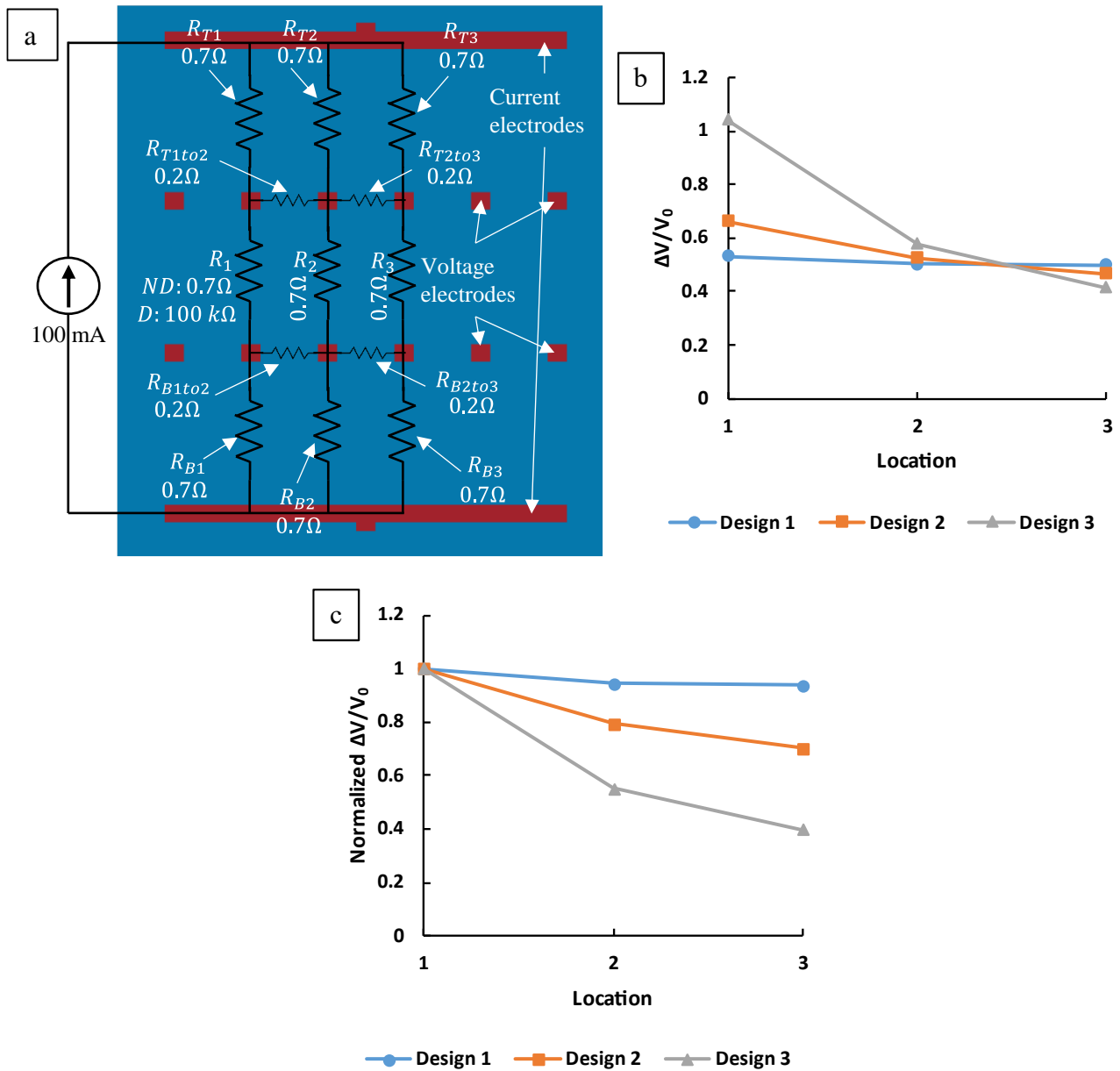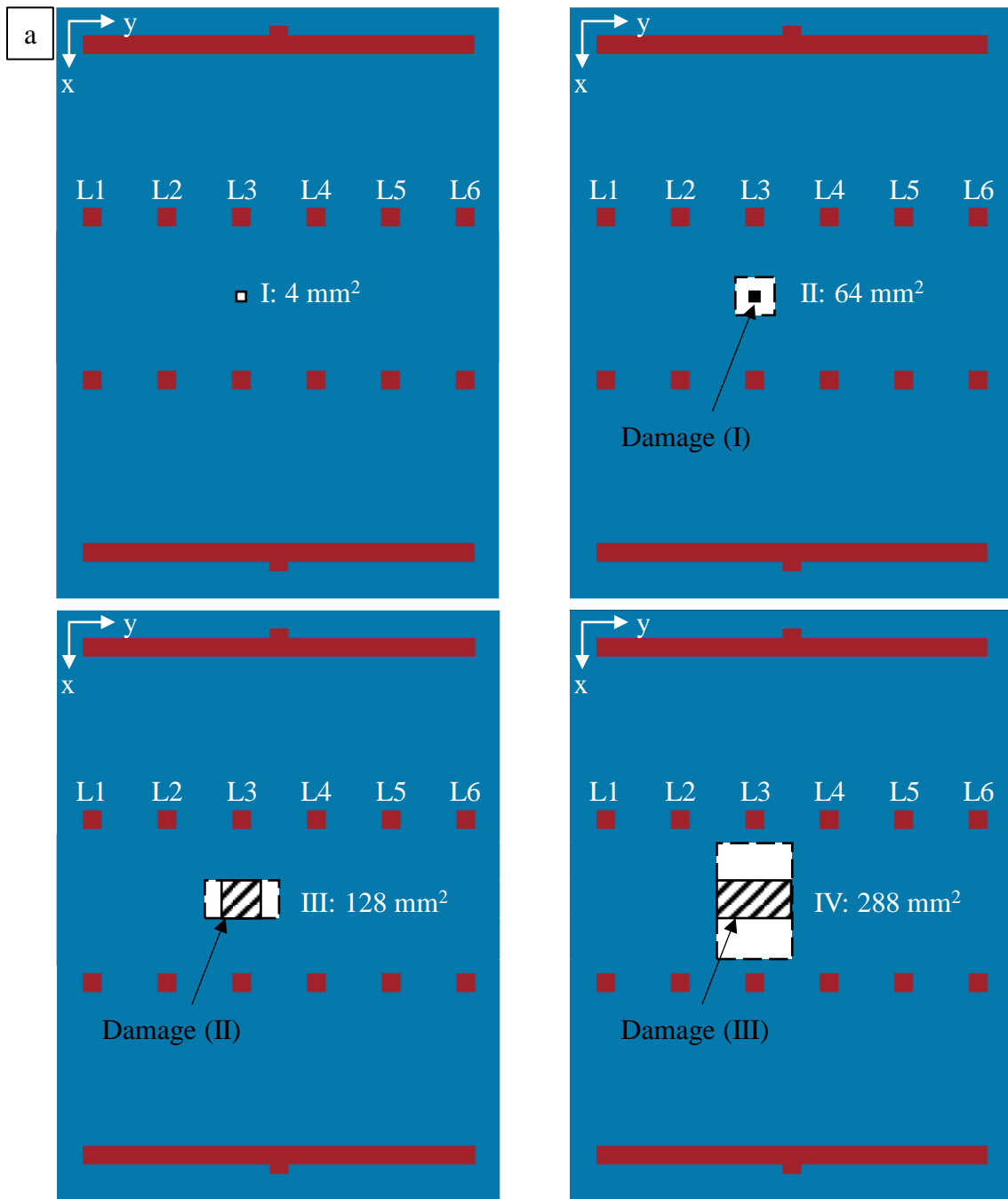
Figure 5. Modeling the carbon fiber damage sensor using lumped resistors. a) The final design of the damage sensor pattern with lumped resistors model. The value of R_1 is ND: No Damage or D: with Damage. b) The percentage voltage change after damage in all three designs. Design 2: Distance between current and voltage electrode rows increased, Design 3: Distance between voltage electrodes is also increased as shown in (a). c) The percentage voltage changes shown in (b) normalized to values between 0 and 1 for each curve for better comparison. The optimized Design 3 shows a clear difference in response between the different electrodes, which means damage location can be detected.

3.2 Testing and Electrical Measurements

The damage sensor was connected to the measurement circuit and measured before and after every individual damage was introduced. The measurement consists of the voltage differences between the top and bottom voltage electrode pairs. The voltage electrode pairs were numbered 1 to 6, corresponding to the locations on the composite. In the first test, the smallest measurable size of damage is determined by applying a small damage in a location and then increasing the damage size in the same location. The same process is then repeated in the next location. Figure 6 (a) shows the order in which damage was applied, which was rectangles of different sizes (I, II, III and IV) in location 3. Then, the same sequence of damage sizes was applied again in each location on the same sample in the order of locations L4, L5 and L2 consecutively. The sizes of the damage rectangles are as follows: (I): 4 mm^2; (II): 64 mm^2; (III): 128 mm^2; (IV): 288 mm^2. Figure 6 (b) shows the percentage increase in voltage using the average of the measurements across all locations for each damage state compared to the voltage in the undamaged state (V_0). This method can be used to estimate the size of the damage applied. The sensor is able to successfully detect all four applied damage sizes by considering each electrode pair individually. The measured voltage change is largest at the location where the damage is applied. This is shown in Figure 6 (c) where damage size (I) was introduced to the same system four times, once in each location in the order L3, L4, L5, L2 resulting in voltage increases by 0.4%, 0.6%, 0.8% and 1.2%, respectively. The difference in voltage increase between locations is due to the previously introduced damage. It is noticed that the larger the existing damage is in the system, the more significant the newly introduced damage's effect will be on voltage because it represents a bigger relative reduction in conductive material from the remaining carbon fiber sheet. The smallest damage size (4 mm^2) can be detected reliably in all cases. To confirm this, a t-test was performed comparing the 50 voltage measurements without and 50 voltage measurements with the 4 mm^2 damage for each electrode pair. The p-value of the test was considerably lower than 0.05 indicating a significant damage-induced voltage change with 95% confidence level. In addition, the error bars for each datapoint in the figures were not included because the standard error was very small so that the error bars would not be visible. As a result, the t-test was used to indicate the stability and reliability of the system. Figure 6 (d) shows the incremental voltage change values normalized between different electrode locations to range from 0 to 1. This is used to identify the newly introduced damage location. The damaged location should exhibit the largest voltage change and thus a normalized value of 1. It can be observed that the voltage changes not only at the damaged location but also to a lesser extent at adjacent locations as expected. This can lead to misidentification of the damage location to an adjacent position if the voltage change is small and there is electrical noise. This is the case the first time damage size (I) was introduced, when there was no other damage present yet. The sensor misplaced the damage from L3 to the adjacent location L2. Conversely, the system locates damage (I) in L4, L5 and L2 successfully. The sensor determines the location of larger damage sizes without any error as shown in Figure 6 (e) where damage size (II) was applied in L3, L4, L5 and L2.
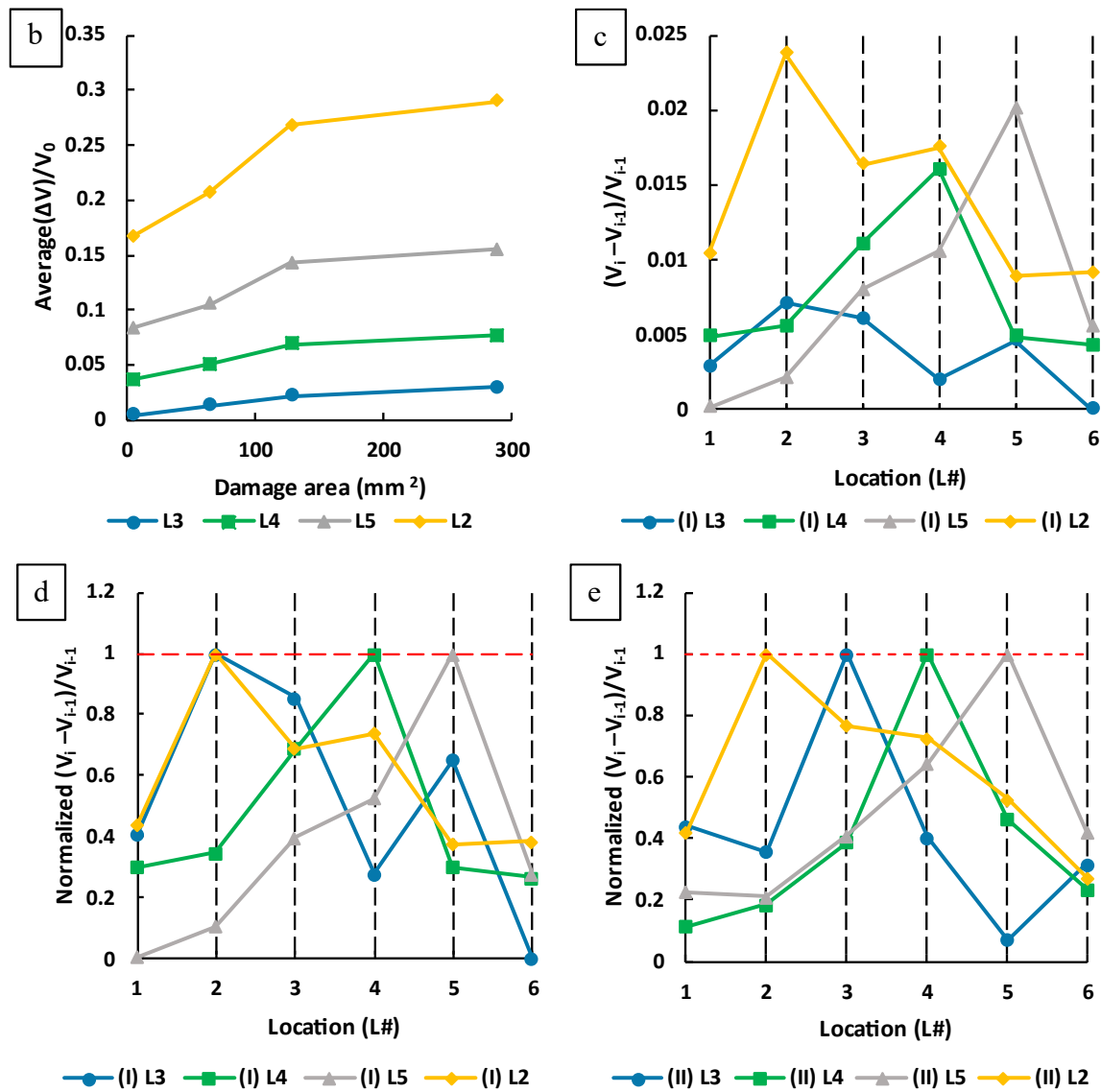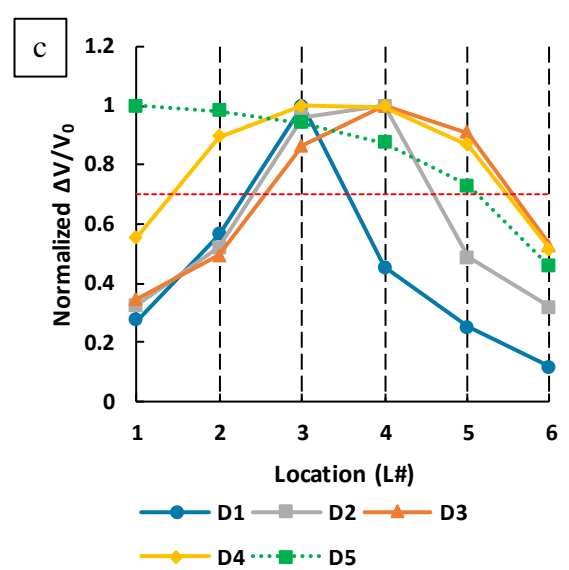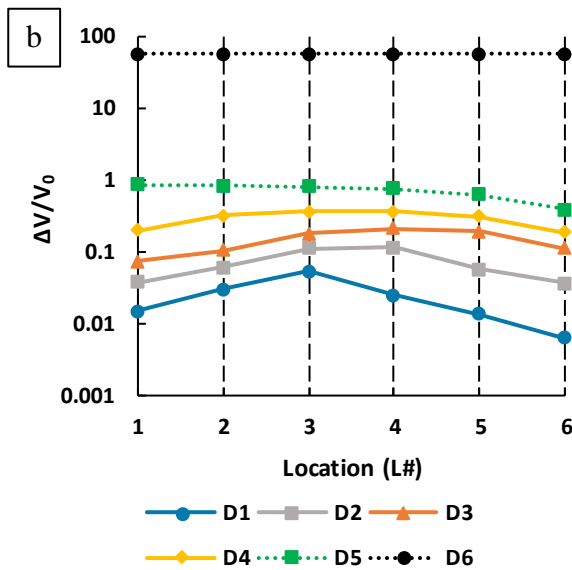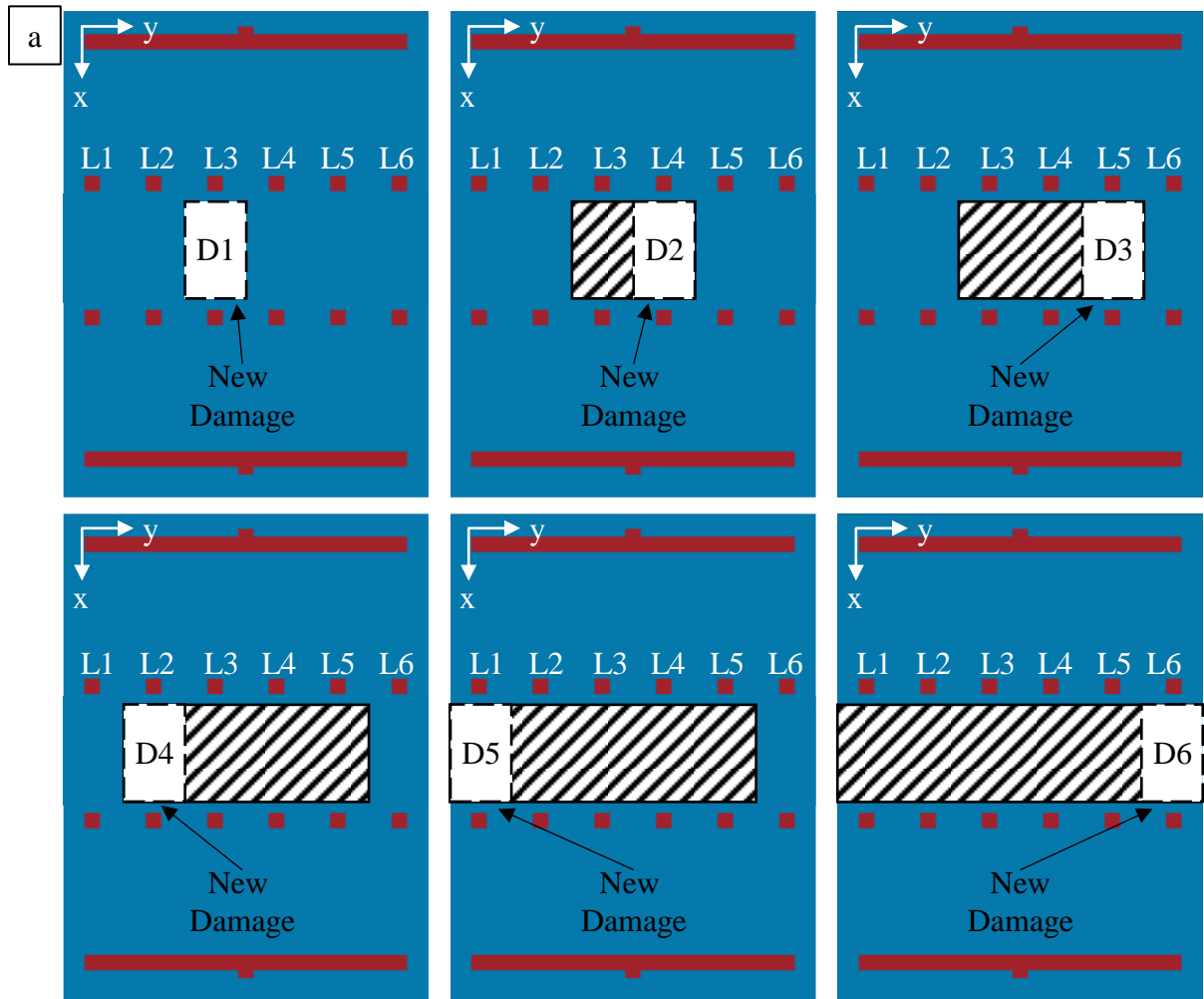
Figure 6. Testing 1D carbon fiber damage sensor in terms of increasing damage size at different locations. a) The drilling pattern in a 1D damage sensor sample proceeding from (I) to (IV) in location 3 (L3). The pattern was repeated in the same order at locations L4, L5 and L2 consecutively. White, non-hatched regions represent newly added damage. b) The percentage increase in voltage across the damage sensor using the average of measurements from all locations for successive measurements in different locations on the same sample. c) Incremental voltage changes between consecutive measurements for the smallest damage size (I). Subscript i-1 denotes voltage measured for the previous damage state. d) Incremental voltage changes for the smallest damage size (I) normalized between electrodes for each curve, showing the locations of newly introduced damage in the composite. The location with the largest voltage change has a value of 1. e) Incremental voltage changes for damage size (II) normalized between electrodes for each curve, showing the locations of newly introduced damage in the composite. The location with the largest voltage change has a value of 1.

In the second test, the location of the newly introduced damage is determined when all introduced damages have the same size. Figure 7 (a) shows a new sample with the same electrode geometry as before, but damage was applied in a different sequence. The damage was applied in increments of damage size IV ($288 \ mm^2$). The damage was drilled in the order shown in the figure from D1 to D6. Figure 7 (b) shows the voltage changes of the system when damage is introduced compared to the undamaged state at each location (V_0). This shows how each damage introduced to the system increases the total resistance of the sensor at all locations. When D6 was drilled, the composite was divided into two completely separated parts, and the voltage measurement was limited by the voltage bounds of the current source. This is an indication that a large enough crack has occurred in the system to completely divide the sensor. To make the damage location clearer, the measured voltage changes for each damage state were normalized between locations from 0 to 1, as shown in Figure 7 (c). This graph can be used to find the extent of the damage that has occurred in the composite. Any locations with a normalized voltage change of more than 70%

are damaged. The same measurements were also compared to the previous measurement every time new damage was introduced to the system and normalized in the same manner, thus showing clearly with a value of 1 where the new damage was introduced, as shown in Figure 7 (d). An Analysis of Variance (ANOVA) test was performed on five samples for this test (shown in Figure 6). It returned a p-value considerably lower than 0.05 indicating that there is no significant difference between the samples and demonstrating the robustness of the approach.
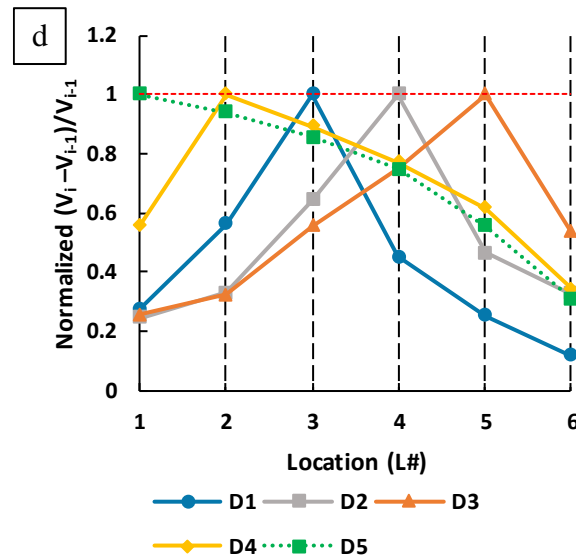
Figure 7. Testing 1D carbon fiber damage sensor in terms of damage location detection. (a) The drilling pattern in a 1D damage sensor sample progressing from D1 to D6. Damage was added cumulatively. White, non-hatched regions represent newly added damage. b) Change in voltage measurements compared to the voltage measurement at the same location before damage was introduced. The voltage increases across the entire sensor with growing damage and the largest voltage increase is found at damaged locations. c) The same data as in (b) but with voltages normalized between electrode locations for each measurement curve. The locations with damage have a normalized value of 0.7 or larger (red dashed line) allowing damaged regions to be identified. d) The same data as in (c) but taking the difference between subsequent measurements. Subscript i-1 denotes voltage measured for previous damage state. The location of newly introduced damage in the composite always exhibits the biggest change normalized to 1.

For comparison, the design previously explored in section 3.1, where the voltage electrodes are closer to each other and closer to the current electrode busses (Design 1), was manufactured and tested. The design and damage drilling patterns are shown in Figure 8 (a). As shown in Figure 8 (b), the sensor does detect damage. However, this design has a lower sensitivity compared to the design previously shown in Figure 6 (a) (Design 3). The smallest damage applied to this design (Figure 8 (a)) was 176 mm^2, which results in a voltage change of 3.6%. Increasing the damage area to 528 mm^2 increases the voltage change by only 0.7% making the total change 4.3%. Conversely, in the previous design (Figure 6 (a)), a 3.7% voltage change is produced by a 292 mm^2 damage area and increasing the damage area to 352 mm^2 increases the voltage change by 1.4%. This means that the optimized design (Figure 6 (a)) can resolve and sense smaller increases in damaged area. This is because the two voltage electrode rows are closer to each other and further from the current electrodes in this design as discussed in section 3.1. In addition, the design that was not optimized could not find the location of the damage at all. This is shown in Figure 8 (c), where the voltage change is compared to the previous state every time new damage is introduced. The data is normalized to values between 0 and 1, making the value 1 the supposed location of the newly introduced damage. When damage (D1) is introduced to the system at location 8, the sensor senses the damage at locations 1, 3, and 6 and completely misses location 8. When (D2) is applied at location 9, the damage is sensed in locations 4 and 10 and completely misses location 9. The sensor also fails to locate the damage in all other locations. This is because, in this design, the voltage electrodes are very close to each other, and the voltage electrode rows are very close to the current electrode busses. This confirms the qualitative insight gained from the lumped resistor model.
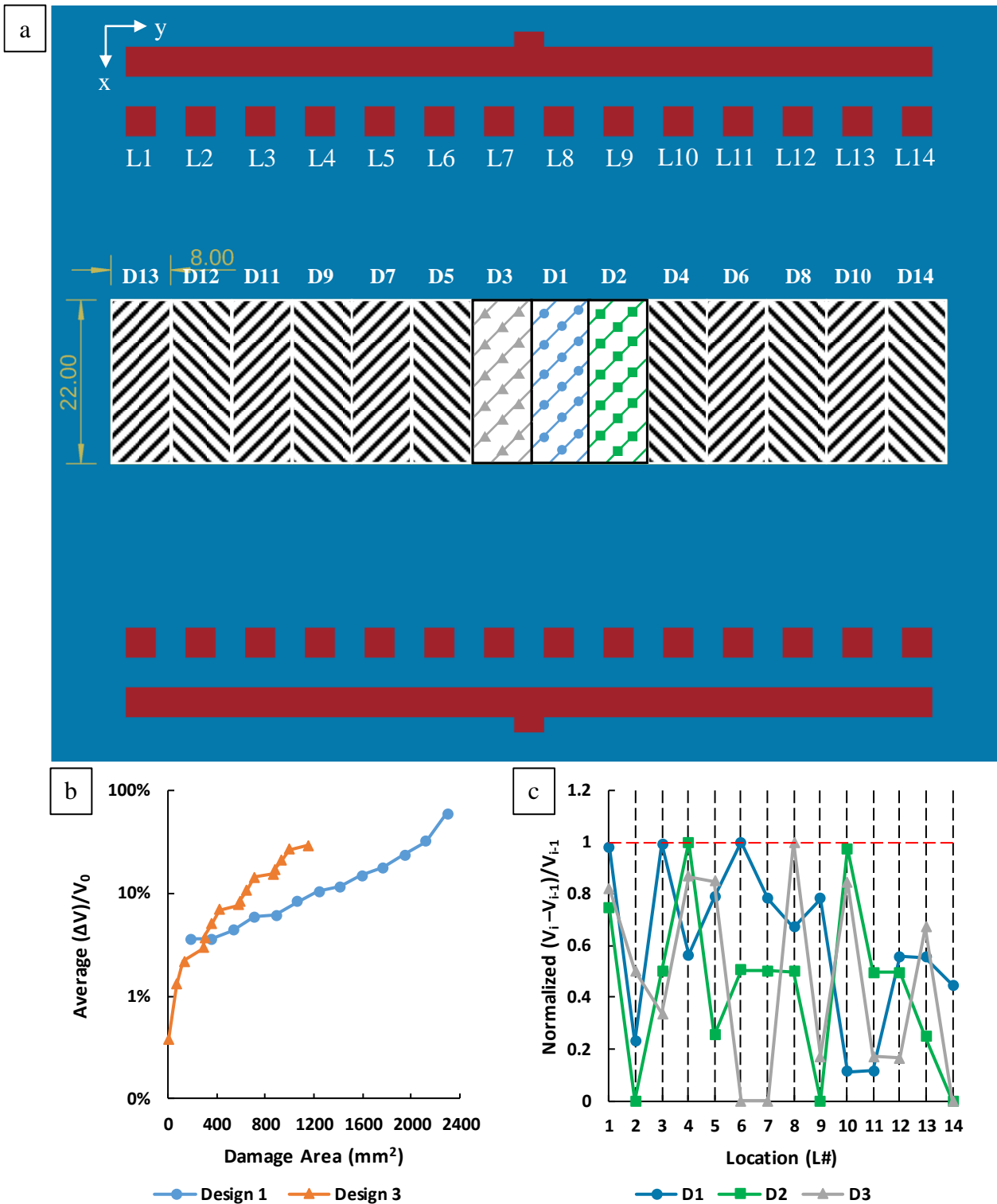
Figure 8. Testing 1D carbon fiber damage sensor (non-optimized Design 1). (a) From 3.1: Design 1 where the voltage electrodes are closer to each other and closer to the current electrode busses. The drilling pattern progresses from D1 to D14. Damage was added cumulatively, e.g. curve D2 in (c) represents damage at locations L3 and L4. Dimensions are in millimeters. b) Percentage increase of measured voltage compared to the voltage measurement before damage was introduced, showing the increase in voltage measurements across the sensor with larger damage. Voltage is the average over all voltage measurement electrodes. Design 3: Final 1D design results included for comparison exhibit a larger sensitivity. c) Normalized percentage increase of voltage compared to the previous voltage measurement showing that the sensor with non-optimized design fails to detect the location of the newly introduced damage.

The same process was applied to the 2D sensor design to locate the damage in both the X- and the Y-direction. This is done by repeating the 1D pattern in multiple rows and locating the damage in each row separately. The top row sensing area was labeled area 1 with damage locations L1 to L6, and the bottom row sensing area was labeled area 2 with damage locations L7 to L12 both from left to right. The damage was applied in order from D1 to D6, as shown in Figure 9 (a). After each damage was applied, the electrical measurements were retaken and normalized, as described previously. Figure 9 (b) shows the simultaneous detection of damage in three separate locations, two (L1, L3) in the top row (area 1) and one (L12) in the bottom row (area 2). The voltage change is larger than 70% in all three locations, thus, the damage locations are detected correctly. Figure 9 (c) and (d) show the normalized percentage voltage change where each measurement is compared to the previous one, thus locating newly introduced damage. This shows that damage can be sensed and located successfully in 2 dimensions.
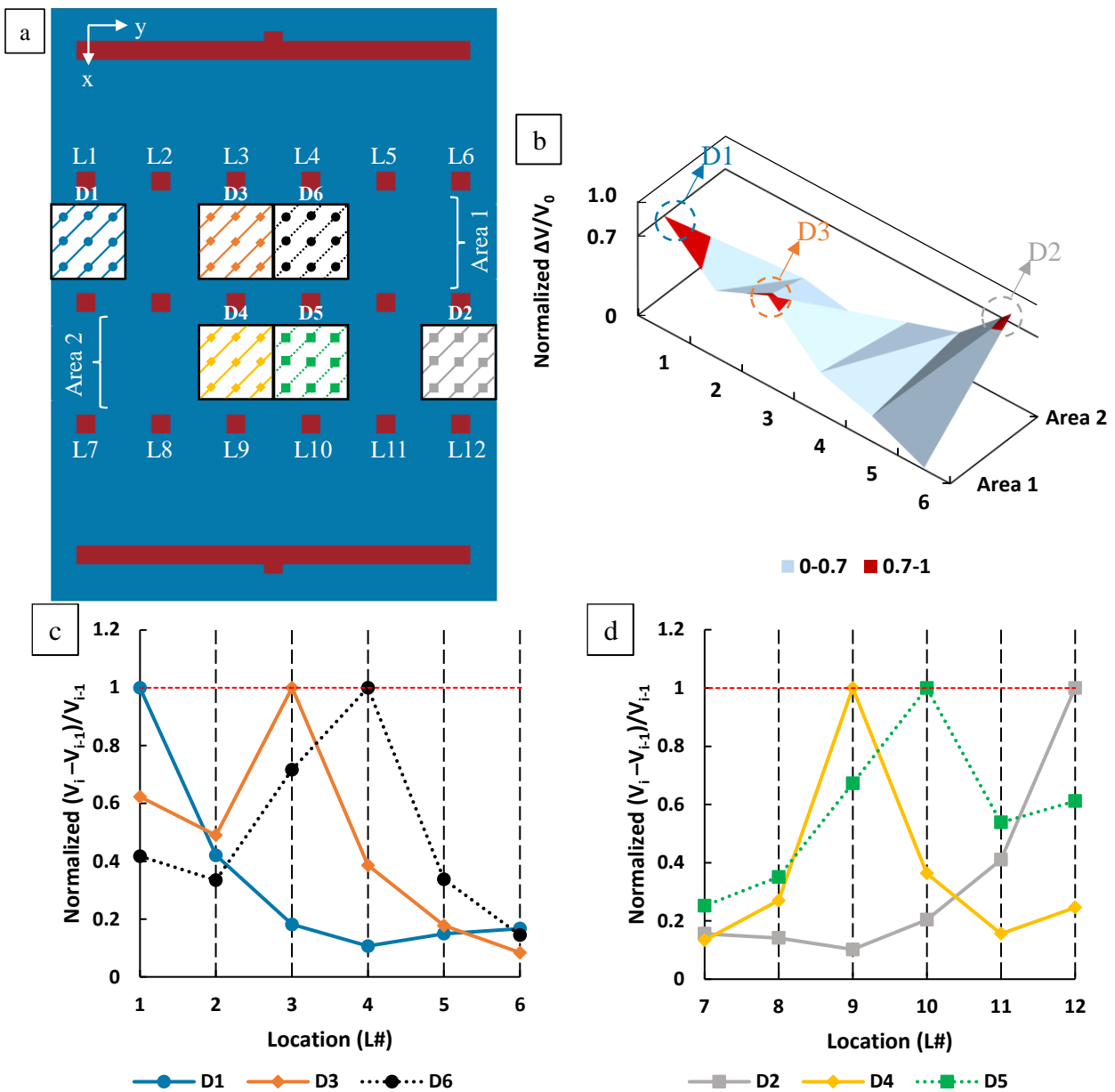

Figure 9. Testing 2D carbon fiber damage sensor. a) The drilling pattern in a 2D damage sensor sample progressing from D1 to D6. b) 3D representation of damage location using the normalized values of the voltage change after D3 was introduced compared to voltage measurements before any damage. The peaks in red correctly identify damages D1 and D3 in locations L1 and L3 in sensing area 1 (top), and damage D2 in location L6 in sensing area 2 (i.e. L12, bottom). c) Normalized percentage voltage change in the top row compared to each previous voltage measurement (subscript i-1) showing the locations of newly introduced damage in this row. Newly created damage leads to the biggest voltage change at the corresponding location as expected (curves normalized to 1). d) The bottom row exhibits the same behavior as the top row when damage is introduced here.

3.3 Simulation Results

To validate the experimental results, the damage sensor was simulated using Sentaurus 2020.09 with and without damage. Figure 10 (a) shows the electrical potential as a function of position in the undamaged sheet. A voltage was applied to the current electrodes inducing current flow from top to bottom. As expected, potential drops from the top to the bottom. Then, damage was introduced as an electrically insulating block in the sensing area. The simulated electrical potential as a function of position is shown in Figure 10 (b). The electrical potential increases in the top voltage measurement electrodes where damage is introduced and decreases in the bottom electrodes. This creates an increase in the voltage difference between the top and bottom electrodes of that location, thus, increasing the resistance of the sheet in that specific area. In addition, damage in a particular location has a small effect on the neighboring locations, and its effect diminishes the farther away the electrodes are from the damage. The value of the electrical potential at the electrode in front of the damage gets closer to the voltage of the closest current electrode as damage size increases until it matches it when the damage divides the sheet completely, as shown with damage D6 in Figure 10 (b). The increase in damage size increases the total resistance of the sheet. The resistance of the damaged sensors was compared to the non-damaged state at the different locations. It was again normalized to a range from 0 to 1 between different electrodes for each experiment as shown in Figure 10 (c). Comparing the plots of damage D1 and D2 from the experimental measurements and the simulation is shown in Figure 10 (d). It is clear that they follow the same trends, and the voltage changes approximately match up. Both experiment and simulation identify the largest resistance change at the location of new damage, which is normalized to 1 in Figure 10 (d). Farther away from the damage location, the average discrepancy between experiment and simulation is 8%. These small differences between the trends could be due to the more complex geometry of the carbon fiber fabric compared to the simulation in Sentaurus, which assumes the material is uniform, disregarding the woven nature of the carbon fiber sheet. Additional factors that may affect the experimental results include measurement errors, contact resistance, or manufacturing errors. However, by using the measurement circuit and normalizing the data as a percentage, the small differences between simulation and experiment are negligible and have no substantial effect on the performance of the sensor.

These simulation results confirm the damage location detection mechanism based on localized voltage measurements in a conductive woven carbon fiber sheet. The simulated potential profiles can be used to refine designs further and decide where to place electrodes in more complex structures.
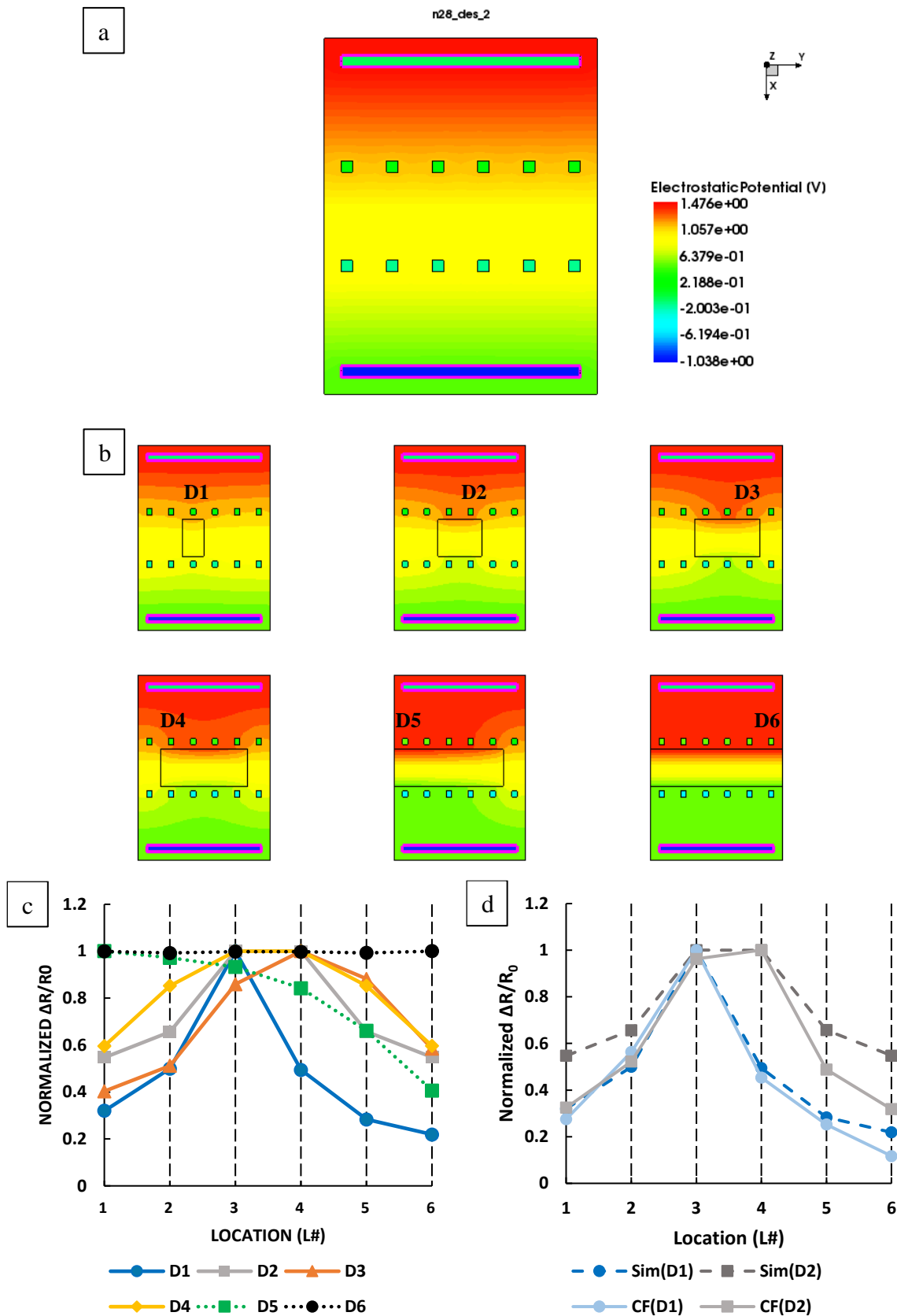
Figure 10. Simulation of 1D damage sensor. a) Electric potential within the undamaged carbon fiber sheet from Sentaurus simulation of 1D damage sensor. b) Sentaurus simulation of 1D damage sensor with different sizes of damage. c) Normalized percentage change in resistance compared to the resistance before damage was introduced. The trends are very similar to the experimental results. d) Comparison of D1 and D2 results between the simulation and the experimental (CF) results showing very good agreement.

3.4 Sensor Characterization and Design Considerations

There are two different modes in which this damage sensor could potentially be operated: analog or digital. In analog mode, the measured voltage values would be converted to the size of the damaged area, which could give better size resolution than the spacing of the electrodes. However, the interpretation of the measured voltage is challenging. The response is highly non-linear, as shown in Figure 6 (b) and Figure 8 (b). The voltage also depends on both x- and y-extent of the damage with different sensitivity. For example, in Figure 6 (b), the voltage increase from damage (II) to (III) is larger than from (III) to (IV) as the sensor is more sensitive to changes in damage size in the y-direction (orthogonal to the direction of current flow) than to changes in the x-direction. Therefore, it is non-trivial to interpret measured voltage values. Further simulations or a priori knowledge of the expected damage, for example cracks in a particular direction, may make it possible to operate the sensor in analog mode. Conversely, operation in digital mode has a lower resolution but is more general and reliable.

In digital mode, each voltage electrode pair is considered as one digital sensor. All electrode pairs' voltage increases from the undamaged state are compared and normalized to values between 0 and 1. All the electrode pairs that have a value above a certain threshold (empirically identified as 0.7 here) are considered damaged. In this way, the resolution in the y-direction corresponds to the spacing between electrodes, which is 16 mm. This is the resolution both in terms of damage location and size. Damage size is estimated as the number of electrodes that show damage multiplied by their spacing. The sensing threshold in terms of damage size is 4 mm^2. This damage size is comparable to literature results for ERT on woven CFRP without printed contacts that identified damage of size 7.1 mm^2 [29], 6.2 mm^2 [30], and 1.2 mm^2 [31] respectively. The accuracy of the sensor in digital mode is limited by its electrode spacing; hence, accuracy is ±8 mm. For the smallest damage that could be detected (4 mm^2), the location error was doubled due to the small induced voltage change leading to damage being identified at the adjacent measurement location. Accuracy could be higher in analog mode; however, this is difficult to interpret as discussed above. The two-dimensional sensor uses another set of electrodes to create a second row of measurement areas. They are evaluated digitally in the same manner to detect if there is damage in an area corresponding to an electrode pair. The resolution and accuracy are again dictated by the spacing between electrodes, now in the x-direction, which is 26 mm here. To improve the resolution, electrodes could potentially be placed closer to each other, and more rows of electrodes could be used. The accuracy reported here is comparable to previous results for woven composites with non-printed contacts that exhibit location error of approximately 10 mm.[29, 30] A recent report used statistical methods to improve location accuracy to 2 mm.[31] Again, these results did not use scalable printing technology, but they show how further improvements in damage detection could be possible with more sophisticated analysis of the measurement data collected with the hardware demonstrated here. However, the resolution (16 mm by 26 mm) and detection threshold (4 mm^2) demonstrated here will be sufficient for many carbon fiber applications to detect damage such as bird strikes, bullet holes, or cracks. These metrics can serve as a starting point for designers when deciding whether to implement this sensing methodology in their carbon fiber composite application. There are a number of design choices and trade-offs that need to be considered, for example, total sensing area, resolution, complexity of the electronics, or smallest damage size that needs to be detected. A designer could explore this space and verify the performance of their design using the finite-element model presented here.

4. Conclusion

This paper presents a 2D digital damage sensing method for woven carbon fiber composites using printed electronics as a scalable manufacturing technology. Conventional composite manufacturing techniques are integrated with the addition of printing electronics on carbon fiber fabric using extrusion printing. Damage is detected by injecting current into the conductive carbon fiber from printed electrodes and measuring voltage at strategic locations with another set of printed electrodes. A circuit that automates switching between electrodes to take high-accuracy measurements and remove contact resistance was designed using a combination of the Kelvin Double Bridge, 4-point probing method, digital multiplexers, and a data acquisition unit. This circuit allows for the scaling of the sensor by merely adding more channels to the multiplexers, thus, enabling the expansion of the sensing area and the increase of spatial resolution as needed. The sensor can successfully detect the size and location of damage in two dimensions. Its resolution is limited by the spacing of the electrodes, which is 16 mm in the y-direction (orthogonal to current flow) and 26 mm in the x-direction. The threshold size of damage that can be detected is 4 mm^2. Different pattern designs were studied experimentally, qualitatively modeled using a lumped resistor model, and simulated using finite-element modeling. The simulation results match the measurement trends with an average difference of 8%. These simulations could be used by designers to adapt the method to the size and shape of their carbon fiber composite application. Further improvements in resolution may also be possible with further optimization; however, the resolution demonstrated here will be sufficient for many applications to detect damage such as bird strikes, bullet holes, or cracks. The resulting damage sensing carbon fiber composite could be integrated into the manufacturing process of composite structures as one of the layers or added

to surfaces of existing large-area structures enabling smart structures and structural health monitoring. In the future, further damage modes could be introduced, for example through tensile tests. Non-destructive evaluation techniques could be used to study such failure and compare the results with electrical measurement and simulations.

Acknowledgements

References

[1]   C. R. Farrar and K. Worden, "An introduction to structural health monitoring," *Philos. Trans. R. Soc. A Math. Phys. Eng. Sci.*, vol. 365, no. 1851, pp. 303–315, Feb. 2007.

[2]   Y. Lingyu and V. Giurgiutiu, "Multi-mode damage detection methods with piezoelectric wafer active sensors," *J. Intell. Mater. Syst. Struct.*, vol. 20, no. 11, pp. 1329–1341, Jul. 2009.

[3]   C. R. Farrar and N. A. J. Lieven, "Damage prognosis: The future of structural health monitoring," *Philos. Trans. R. Soc. A Math. Phys. Eng. Sci.*, vol. 365, no. 1851, pp. 623–632, Feb. 2007.

[4]   Z. Wan, J. D. Li, M. Jia, and J. L. Li, "Structural health monitoring (SHM) of three-dimensional braided composite material using carbon nanotube thread sensors," *J. Mech.*, vol. 29, no. 4, pp. 617–621, 2013.

[5]   J. M. Ko and Y. Q. Ni, "Technology developments in structural health monitoring of large-scale bridges," *Eng. Struct.*, vol. 27, no. 12 SPEC. ISS., pp. 1715–1725, Oct. 2005.

[6]   A. C. Douglass and J. B. Harley, "Model-based statistical guided wave damage detection for an aluminum plate," *Struct. Heal. Monit.*, p. 147592172090950, Mar. 2020.

[7]   A. N. Zagrai and V. Giurgiutiu, "Electro-Mechanical Impedance Method for Crack Detection in Thin Plates," *J. Intell. Mater. Syst. Struct.*, vol. 12, no. 10, pp. 709–718, Oct. 2001.

[8]   V. Giurgiutiu, A. Zagrai, and J. Bao, "Damage identification in aging aircraft structures with piezoelectric wafer active sensors," in *Journal of Intelligent Material Systems and Structures*, 2004, vol. 15, no. 9–10, pp. 673–687.

[9]   I. Perez-Alfaro, D. Gil-Hernandez, O. Muñoz-Navascues, J. Casbas-Gimenez, J. C. Sanchez-Catalan, and N. Murillo, "Low-cost piezoelectric sensors for time domain load monitoring of metallic structures during operational and maintenance processes," *Sensors (Switzerland)*, vol. 20, no. 5, Mar. 2020.

[10]   M. S. Scholz *et al.*, "The use of composite materials in modern orthopaedic medicine and prosthetic devices: A review," *Composites Science and Technology*, vol. 71, no. 16. Elsevier, pp. 1791–1803, 14-Nov-2011.

[11]   B. A. Newcomb, "Processing, structure, and properties of carbon fibers," *Composites Part A: Applied Science and Manufacturing*, vol. 91. Elsevier Ltd, pp. 262–282, 01-Dec-2016.

[12]   I. Jerkovic, V. Koncar, and A. Grancaric, "New Textile Sensors for In Situ Structural Health Monitoring of Textile Reinforced Thermoplastic Composites Based on the Conductive Poly(3,4-ethylenedioxythiophene)-poly(styrenesulfonate) Polymer Complex," *Sensors*, vol. 17, no. 10, p. 2297, Oct. 2017.

[13]   X. Fu and D. D. L. Chung, "Self-monitoring of fatigue damage in carbon fiber reinforced cement," *Cem. Concr. Res.*, vol. 26, no. 1, pp. 15–20, Jan. 1996.

[14]   X. Wang, S. Wang, and D. D. L. Chung, "Sensing damage in carbon fiber and its polymer-matrix and carbon-matrix composites by electrical resistance measurement," *J. Mater. Sci.*, vol. 34, no. 11, pp. 2703–2713, 1999.

[15]   S. Wen and D. D. L. Chung, "Electrical-resistance-based damage self-sensing in carbon fiber reinforced cement," *Carbon N. Y.*, vol. 45, no. 4, pp. 710–716, Apr. 2007.

[16]   S. Wang and D. D. L. Chung, "Self-sensing of flexural strain and damage in carbon fiber polymer-matrix composite by electrical resistance measurement," *Carbon N. Y.*, vol. 44, no. 13, pp. 2739–2751, Nov. 2006.

[17]   L. Gao, E. T. Thostenson, Z. Zhang, and T. W. Chou, "Sensing of damage mechanisms in fiber-reinforced composites under cyclic loading using carbon nanotubes," *Adv. Funct. Mater.*, vol. 19, no. 1, pp. 123–130, Jan. 2009.

[18]   Y. Okabe, N. Tanaka, and N. Takeda, "Effect of fiber coating on crack detection in carbon fiber reinforced plastic composites using fiber Bragg grating sensors," *Smart Mater. Struct.*, vol. 11, no. 6, p. 892, Oct. 2002.

[19]   L. Cheng and G. Y. Tian, "Surface crack detection for carbon fiber reinforced plastic (CFRP) materials using pulsed eddy current thermography," *IEEE Sens. J.*, vol. 11, no. 12, pp. 3261–3268, 2011.

[20]   Y. Okabe, S. Yashiro, T. Kosaka, and N. Takeda, "Detection of transverse cracks in CFRP composites using embedded fiber Bragg grating sensors," *Smart Mater. Struct.*, vol. 9, no. 6, p. 832, 2000.

[21]   C. Cherif, E. Haentzsche, R. Mueller, A. Nocke, M. Huebner, and M. M. B. Hasan, "Carbon fibre sensors embedded in glass fibre-based composites for windmill blades," *Smart Text. Their Appl.*, pp. 329–352, 2016.

[22]   J. Qiu, M. K. Idris, G. Grau, and G. W. Melenka, "Fabrication of electroluminescent carbon fiber composite for damage visualization," *Manuf. Lett.*, vol. 24, pp. 56–60, Apr. 2020.

[23]   R. Schueler, S. P. Joshi, and K. Schulte, "Damage detection in CFRP by electrical conductivity mapping," *Compos. Sci. Technol.*, vol. 61, no. 6, pp. 921–930, May 2001.

[24]   L. C. Masson and P. E. Irving, "Comparison of experimental and simulation studies of location of impact damage in polymer composites using electrical potential techniques," *https://doi.org/10.1117/12.396399*, vol. 4073, pp. 182–193, Aug. 2000.

[25]   A. Todoroki, Y. Tanaka, and Y. Shimamura, "Multi-prove electric potential change method for delamination monitoring of graphite/epoxy composite plates using normalized response surfaces," *Compos. Sci. Technol.*, vol. 64, no. 5, pp. 749–758, Apr. 2004.

[26]   N. Angelidis, N. Khemiri, and P. E. Irving, "Experimental and finite element study of the electrical potential technique for damagedetection in CFRP laminates," *Smart Mater. Struct.*, vol. 14, no. 1, p. 147, Dec. 2004.

[27]   D. Wang, S. Wang, D. D. L. Chung, and J. H. Chung, "Comparison of the Electrical Resistance and Potential Techniques for the   Self-sensing of Damage in Carbon Fiber Polymer-Matrix Composites:," *http://dx.doi.org/10.1177/1045389X06060218*, vol. 17, no. 10, pp. 853–861, Jul. 2016.

[28]   L. W. E. Galvis, P. Diaz-Montiel, and S. Venkataraman, "Optimal Electrode Selection for Electrical Resistance Tomography in Carbon Fiber Reinforced Polymer Composites," *Mater. 2017, Vol. 10, Page 125*, vol. 10, no. 2, p. 125, Feb. 2017.

[29]   A. Baltopoulos, N. Polydorides, L. Pambaguian, A. Vavouliotis, and V. Kostopoulos, "Damage identification in carbon fiber reinforced polymer plates using electrical resistance tomography mapping:," *http://dx.doi.org/10.1177/0021998312464079*, vol. 47, no. 26, pp. 3285–3301, Oct. 2012.

[30]   J. Cagáň, "Hardware implementation of electrical resistance tomography for damage detection of carbon fibre–reinforced polymer composites:," *http://dx.doi.org/10.1177/1475921716666004*, vol. 16, no. 2, pp. 129–141, Sep. 2016.

[31]   J. Cagáň and L. Michalcová, "Impact Damage Detection in CFRP Composite via Electrical Resistance Tomography by Means of Statistical Processing," *J. Nondestruct. Eval. 2020 392*, vol. 39, no. 2, pp. 1–12, Apr. 2020.

[32]   J. S. Chang, A. F. Facchetti, and R. Reuss, "A Circuits and Systems Perspective of Organic/Printed Electronics: Review, Challenges, and Contemporary and Emerging Design Approaches," *IEEE J. Emerg. Sel. Top. Circuits Syst.*, vol. 7, no. 1, pp. 7–26, Mar. 2017.

[33]   H. F. Castro *et al.*, "Degradation of all-inkjet-printed organic thin-film transistors with TIPS-pentacene under processes applied in textile manufacturing," *Org. Electron.*, vol. 22, pp. 12–19, Jul. 2015.

[34]   Y. Khan, A. Thielens, S. Muin, J. Ting, C. Baumbauer, and A. C. Arias, "A New Frontier of Printed Electronics: Flexible Hybrid Electronics," *Adv. Mater.*, p. 1905279, Nov. 2019.

[35]   T. Augustin, D. Grunert, H. H. Langner, V. Haverkamp, and B. Fiedler, "Online monitoring of surface cracks and delaminations in carbon fiber/epoxy composites using silver nanoparticle based ink," *Adv. Manuf. Polym. Compos. Sci.*, vol. 3, no. 3, pp. 110–119, Jul. 2017.

[36]   F. Heinrich, T. Genco, and R. Lammering, "On the mechanical behavior of a composite stiffener with inkjet-printed electronics," in *9th European Workshop on Structural Health Monitoring, EWSHM 2018*, 2018.

[37]   F. Heinrich and R. Lammering, "A numerical approach to simulate printed electronics on fiber reinforced composites," *PAMM*, vol. 16, no. 1, pp. 135–136, Oct. 2016.

[38]   F. Heinrich and R. Lammering, "An experimental investigation on the adhesion of printed electronics on fiber reinforced composites," in *8th European Workshop on Structural Health Monitoring, EWSHM 2016*, 2016, vol. 4, pp. 2949–2956.

[39]   F. Heinrich, H. H. Langner, and R. Lammering, "On the identification of cohesive parameters for printed metal-polymer interfaces," *Smart Mater. Struct.*, vol. 26, no. 5, p. 055025, Apr. 2017.

[40]   E. B. Jeon, T. Fujimura, K. Takahashi, and H. S. Kim, "An investigation of contact resistance between carbon fiber/epoxy composite laminate and printed silver electrode for damage monitoring," *Compos. Part A Appl. Sci. Manuf.*, vol. 66, pp. 193–200, Nov. 2014.

[41]   S. J. Joo, M. H. Yu, E. B. Jeon, and H. S. Kim, "In situ fabrication of copper electrodes on carbon-fiber-reinforced polymer (CFRP) for damage monitoring by printing and flash light sintering," *Compos. Sci. Technol.*, vol. 142, pp. 189–197, Apr. 2017.

[42]   M. Stoppa and A. Chiolerio, "Wearable electronics and smart textiles: A critical review," *Sensors (Switzerland)*, vol. 14, no. 7. pp. 11957–11992, 07-Jul-2014.

[43]   M. G. Mohammed and R. Kramer, "All-Printed Flexible and Stretchable Electronics," *Adv. Mater.*, vol. 29, no. 19, May 2017.

[44]   M. S. Rahman and G. Grau, "Direct writing of stretchable metal flake conductors: improved stretchability and conductivity by combining differently sintered materials," *Flex. Print. Electron.*, Apr. 2020.

[45]   K. Suganuma, "Printing Technology," 2014, pp. 23–48.

[46]   K. B. Perez and C. B. Williams, "Combining additive manufacturing and direct write for integrated electronics - A review," in *24th International SFF Symposium - An Additive Manufacturing Conference, SFF 2013*, 2013, pp. 962–979.

[47]   S. Khan, L. Lorenzelli, and R. S. Dahiya, "Technologies for printing sensors and electronics over large flexible substrates: A review," *IEEE Sens. J.*, vol. 15, no. 6, pp. 3164–3185, Jun. 2015.

[48]   K.-S. Kwon, M. K. Rahman, T. H. Phung, S. D. Hoath, S. Jeong, and J. S. Kim, "Review of digital printing technologies for electronic materials," *Flex. Print. Electron.*, vol. 5, no. 4, p. 043003, Dec. 2020.

[49]   M. K. Idris, J. Qiu, G. W. Melenka, and G. Grau, "Printing electronics directly onto carbon fiber composites: unmanned aerial vehicle (UAV) wings with integrated heater for de-icing," *Eng. Res. Express*, vol. 2, no. 2, p. 025022, May 2020.

[50]   C. Jooss *et al.*, "The 100th anniversary of the four-point probe technique: The role of probe geometries in isotropic and anisotropic systems," *J. Phys. Condens. Matter*, vol. 27, no. 22, p. 223201, 2015.

[51]   A. Horoschenkoff and C. Christner, "Carbon Fibre Sensor : Theory and Application," *In-Tech*, pp. 1–20, Aug. 2012.

[52]   S. Singh, N. Kumar, and A. Monga, "To implement resistance measurement techniques using DC bridge circuits (Wheatstone and Kelvin double bridge) on National Instruments ELVIS-II workstation," *Int. J. Adv. Res. Comput.*

Eng. Technol., vol. 4, no. May, pp. 1686–1690, 2015.